

Load simulation and local dynamics of support structures for offshore wind turbines

Von der
Fakultät für Bauingenieurwesen und Geodäsie
der
Gottfried Wilhelm Leibniz Universität Hannover
zur Erlangung des Grades eines

Doktors der Ingenieurwissenschaften

- Dr.-Ing. -

genehmigte Dissertation
von

Dipl.-Ing. Cord Böker
geboren am 18.09.1976 in Hannover.

2009

Promotionskommission:

Hauptreferent: Prof. Dr.-Ing. Peter Schaumann

Korreferent: Prof. Dr. Dipl.-Ing. Martin Kühn

Kommissionsmitglied: Prof. Dr.-Ing. habil. Raimund Rolfes

Vorsitzender: Prof. Dr.-Ing. Ludger Lohaus

Tag der Promotion: 21. August 2009

Schriftenreihe des Instituts für Stahlbau
der Gottfried Wilhelm Leibniz Universität Hannover

Heft 26

Cord Böker

**Load simulation and local dynamics of support structures
for offshore wind turbines**

Shaker Verlag
Aachen 2010

Bibliographic information published by the Deutsche Nationalbibliothek

The Deutsche Nationalbibliothek lists this publication in the Deutsche Nationalbibliografie; detailed bibliographic data are available in the internet at <http://dnb.d-nb.de>.

Zugl.: Hannover, Leibniz Univ., Diss., 2009

Herausgeber:

Prof. Dr.-Ing. Peter Schaumann

Institut für Stahlbau

Appelstr. 9A

30167 Hannover

<http://www.stahlbau.uni-hannover.de>

Copyright Shaker Verlag 2010

All rights reserved. No part of this publication may be reproduced, stored in a retrieval system, or transmitted, in any form or by any means, electronic, mechanical, photocopying, recording or otherwise, without the prior permission of the publishers.

Printed in Germany.

ISBN 978-3-8322-8850-1

ISSN 1617-8327

Shaker Verlag GmbH • P.O. BOX 101818 • D-52018 Aachen

Phone: 0049/2407/9596-0 • Telefax: 0049/2407/9596-9

Internet: www.shaker.de • e-mail: info@shaker.de

Executive Summary

The installation of the German offshore test field *alpha ventus* in the North Sea marks the beginning of a new era of offshore wind energy application. Fueled by European renewable energy targets and the increasing reliability of the technology, offshore wind energy has become a multi-billion euro market that attracts the interest of many stakeholders. Consequently, there is a potential of rapid growth of that market over the next decade.

The successful deployment of offshore wind turbines in a large scale will require innovative, lightweight, safe, and cost-effective support structures. For the severe North Sea conditions in water depths around 30m and more, braced or lattice support structures like tripod or jacket seem to be the preferred solution. Taking into account the dynamic interrelation of those support structures and their internal dynamics with the wind turbine in numerical models for dynamic simulations becomes crucial for a reliable and cost-effective design.

Therefore, in this thesis a new analysis approach is implemented and verified that takes the complete offshore wind turbine consisting of rotor nacelle assembly, tower, and substructure into account. This is achieved by coupling Poseidon, a finite element code specifically designed for the simulation of lattice offshore support structures by the author, to the quasi-industry standard wind turbine simulation code Flex5, which was available to the author in the version of the Endowed Chair of Wind Energy at the University of Stuttgart.

In lack of measurement data from real turbines with complex support structures the simulation results of the international benchmarking project OC3 have been used to verify the approach. Very good agreement with the results of other codes participating in that project could be achieved. The turbine model that is used within OC3, the NREL 5MW Baseline Turbine, is taken as reference turbine for the further investigations in the thesis, too.

The approach is applied to investigate the excitation of local vibrations of support structures for offshore wind turbines in combined aero-servo-hydro-elastic simulations. The parameters that influence the local dynamics are analyzed separately by means of coupled modal analysis at the example of a reference jacket. In subsequent coupled analyses in the time domain it can be shown how local vibrations of the braces of the jacket are excited by coupling effects between local brace modes with modes of the rotor nacelle assembly.

Based on the analyses it is concluded that particularly structures with internal modes at comparatively low eigenfrequencies are prone to excitation of local vibrations due to coupling effects. It is therefore recommended to identify potential sources of resonance by means of coupled modal analysis. Potential savings in the detailed structural design will pay off the additional computational effort required for fully coupled analyses in case significant contribution from local vibrations is to be expected.

Kurzzusammenfassung

Mit der Errichtung des Offshore Testfelds *alpha ventus* in der Deutschen Nordsee beginnt ein neues Zeitalter der Windenergienutzung. Angetrieben durch europäische Vereinbarungen zum Ausbau der Erneuerbaren Energien und durch die zunehmende Zuverlässigkeit dieser Technologie ist die Offshore Windenergie zu einem Multi-Milliarden Euro Markt herangewachsen der in den kommenden Jahren ein enormes Wachstumspotenzial aufweist.

Um Offshore Windenergieanlagen im großen Maßstab errichten zu können, werden innovative, leichte, sichere und wirtschaftliche Tragstrukturen für diese Anlagen benötigt. Für die Standorte in der Nordsee mit Wassertiefen von 30m und mehr sind so genannte aufgelöste Tragstrukturen wie der Tripod oder das Jacket die bevorzugten Varianten. Die Betrachtung der wechselseitigen Beeinflussung zwischen Windenergieanlage und Tragstruktur sowie deren interner Dynamik ist unabdingbar für eine zuverlässige und wirtschaftliche Bemessung.

In dieser Arbeit wird daher ein neuer Lösungsansatz implementiert und verifiziert, in dem die gesamte Offshore Windenergieanlage bestehend aus Rotor-Gondel-Einheit, Turm und Substruktur in Betracht gezogen wird. Dazu wird das vom Verfasser entwickelte Programm Poseidon, ein Finite-Elemente-Programm speziell für die Simulation von aufgelösten Offshore-Strukturen, mit dem weit verbreiteten Windenergieanlagensimulationsprogramm Flex5 gekoppelt, welches in der Version des Stiftungslehrstuhls Windenergie der Universität Stuttgart zur Verfügung stand.

Der Ansatz wird anhand von Ergebnissen des internationalen Benchmarking Projekts OC3 verifiziert. Es kann eine sehr gute Übereinstimmung mit den Ergebnissen anderer Simulationsprogramme, die in dem Projekt vertreten sind, erreicht werden. Das Modell der Windenergieanlage, das für die Berechnungen in OC3 verwendet wird, die NREL 5MW Baseline Turbine, wird auch für die weiteren Berechnungen als Referenzanlage herangezogen.

Der Ansatz wird verwendet, um die Anregung lokaler Schwingungen der Tragstrukturen unter kombinierter aero-servo-hydro-dynamischer Beanspruchung zu untersuchen. Die das lokale Schwingverhalten beeinflussenden Parameter werden separat mit Hilfe gekoppelter Modalanalysen am Beispiel eines Referenz-Jackets analysiert. In anschließenden Zeitbereichsanalysen wird gezeigt, wie lokale Schwingungen durch Koppelungseffekte zwischen den inneren Moden des Jackets und den Blättern der Windenergieanlage angeregt werden.

Auf der Grundlage der Untersuchungen wird festgestellt, dass insbesondere Strukturen mit inneren Moden vergleichsweise niedriger Eigenfrequenzen zu durch Kopplungseffekte verursachten lokalen Schwingungen neigen. Es wird daher empfohlen, potentielle Resonanzquellen frühzeitig durch gekoppelte Modalanalysen zu identifizieren. Die so erzielten Materialeinsparungen werden den zusätzlichen rechnerischen Aufwand für eine voll gekoppelte Analyse aufwiegen.

Acknowledgements

The work presented in this thesis was carried out while I was employed at the Institute for Steel Construction of the Leibniz Universität Hannover from 2004-2009. First of all, I would like to express my gratitude to the supervisor of my PhD and principle referee Prof. Dr.-Ing. Peter Schaumann for the support of my work and for the encouraging atmosphere at the institute. Furthermore, I would like to thank Prof. Dr. Dipl.-Ing. Martin Kühn for acting as co-referee.

While I was employed at the institute I was financially supported by the German Federal Ministry for the Environment, Nature Conservation and Nuclear Safety (BMU) within the research projects “Validierung bautechnischer Bemessungsmethoden für Offshore-Windenergieanlagen anhand der Messdaten der Messplattformen FINO 1 und FINO 2 (GIGAWINDplus, FKZ 0329944)” and “Verifikation von Offshore-Windenergieanlagen (OWEA, FKZ 0327696)”, which formed a basis for the work carried out in the thesis.

The development of Poseidon started back in 2005 together with Dipl.-Ing. Ralf Schüttendiebel, whom I would like to thank for two incredibly productive months and many good ideas. Similarly, I would like to thank Dipl.-Ing. Daniel Kaufer for the fun we had during the implementation phase of the Flex5-Poseidon coupling and for the many fruitful discussions since then. I would also like to acknowledge the contribution of Dr.-Ing. Marc Seidel and Dipl.-Ing. Nicolai Cosack who provided insights in the mysteries of Flex5 as well as they were general ping-pong partners for discussions on simulation of offshore wind turbines. Speaking of Flex5, I would like to thank the Endowed Chair of Wind Energy of the University of Stuttgart for making it possible to use their version of Flex5 for the work carried out in this thesis.

I would like to thank the colleagues at the institute for their creating an excellent work atmosphere and their support. Particularly, I would like to thank Dr.-Ing. Christian Keindorf for the encouragement to actually open “the document” during the ISOPE conference in Vancouver in 2008. Also, I would like to thank Dipl.-Ing. Fabian Wilke for the inspiring collaboration. I will ever keep in mind last-minute accomplishments, e.g. at the occasion of DEWEK 2006. A tradition, by the way, that is greatly being continued by Dipl.-Ing. Stephan Lochte-Holtgreven, whom I also would like to thank.

I would like to thank Dipl.-Ing. Dipl.-Wirtsch.-Ing. Thorsten Schnieders for carefully reading the thesis and giving many good recommendations.

Finally, it is hard to find words to express my gratitude to my wife Maike for her moral support and for her patience and for her understanding during the last years. Our children Joris and Henrike also contributed to the successful completion of this work by enriching my life in general and keeping me grounded.

Contents

1. INTRODUCTION	1
1.1 Motivation and background	1
1.2 Objectives and structure of the thesis	3
2. LOADING OF OFFSHORE WIND TURBINES	4
2.1 Load assumptions for offshore wind turbines	4
2.1.1 Wind loads	5
2.1.2 Wave loads	7
2.1.3 Joint distribution of wind and waves	17
2.1.4 Dynamic loading	17
2.2 Harmonic excitation of structures	19
2.2.1 Dynamic amplification	19
2.2.2 Campbell Diagram	21
3. LOAD SIMULATION OF OFFSHORE WIND TURBINES	23
3.1 Reduction methods	23
3.1.1 Static condensation	23
3.1.2 Guyan Reduction	24
3.1.3 Modal condensation	25
3.2 Simulation approaches for OWT	26
3.2.1 Superposition method	27
3.2.2 Semi-integrated approach	28
3.2.3 Sequential Approach	29
3.2.4 Full coupling	30
3.2.5 Fully integrated approach	32
3.3 Simulation codes	32
4. DEVELOPMENT OF A FINITE ELEMENT CODE FOR SUPPORT STRUCTURES OF OFFSHORE WIND TURBINES	36
4.1 General features of the FE-code Poseidon	36
4.2 Wave and sea state loading	40
4.3 Time domain simulation	43
4.4 Postprocessing	47
5. COUPLING OF FLEX5 AND POSEIDON	50
5.1 Outline of the coupling approach	50
5.1.1 Structural modeling in Flex5	50
5.1.2 Global equation system	52

5.2	Implementation of the full coupling	54
5.2.1	Communication protocol	54
5.2.2	Coordinate transformation	54
5.2.3	Damping	56
5.2.4	Coupled modal analysis	57
5.2.5	Time domain simulation	57
5.3	Implementation of the sequential approach	59
5.4	Evaluation of the Flex5-Poseidon-Coupling	60
6.	REFERENCES FOR SIMULATIONS	63
6.1	NREL 5MW Baseline Turbine	63
6.2	Reference support structures	66
6.2.1	OC3 Phase I Monopile	66
6.2.2	Tripod	68
6.2.3	Jacket	71
6.3	Design Basis	75
7.	VERIFICATION OF THE FLEX5-POSEIDON-COUPLING	77
7.1	Verification of the stand-alone simulation capabilities of Poseidon	77
7.1.1	Wave loads	77
7.1.2	Comparison with measurement data	79
7.2	Model check – static equilibrium	83
7.3	Benchmarking against OC3 results	85
7.3.1	Phase I – Monopile	85
7.3.2	Phase III – Tripod	97
8.	INFLUENCES ON THE LOCAL DYNAMICS	102
8.1	Introduction - vibrations of a simple beam	102
8.2	Modal analysis of the reference jacket	103
8.3	Added Masses	106
8.3.1	Hydrodynamic added mass	106
8.3.2	Marine growth	107
8.3.3	Application to the jacket model	109
8.4	Local Joint Flexibility	112
8.4.1	General	113
8.4.2	Application to the jacket model	118
8.5	Hydrodynamic damping	120
8.6	Local dynamics in the sequential approach	123
8.6.1	Review of the Guyan reduction method	123
8.6.2	Influence on the local dynamics	125
8.6.3	Application to the jacket model	129
9.	EXCITATION OF LOCAL VIBRATIONS	131
9.1	Load cases for time domain simulations	131
9.2	Time domain simulations	132
9.2.1	Deterministic loading	133
9.2.2	Stochastic loading from wind	136
9.2.3	Combined wind and wave loading	138

9.3 Comparison of full coupling and sequential approach	140
9.3.1 Investigations related to the jacket model	141
9.3.2 Evaluation for different substructure types	144
10. CONCLUSIONS AND RECOMMENDATIONS	146
REFERENCES	149
APPENDIX A GEOMETRY OF THE REFERENCE JACKET	153
APPENDIX B ELEMENT MATRICES USED IN POSEIDON	160
B.1 Truss Elements and springs	160
B.2 Beam Elements	161
B.3 Mass Elements	164
B.4 Damper Elements	164
CURRICULUM VITAE	165

List of Tables

Table 1: Approved offshore projects in the German exclusive economic zone	1
Table 2: Wind turbine classes acc. to IEC 61400-1 Ed.3.....	6
Table 3: Overview of existing wind turbine simulation codes with respective aero-hydro-servo-elastic modeling capabilities	35
Table 4: Comparison of simulation speeds for different configurations.....	62
Table 5: Main properties of the NREL 5MW Baseline Turbine	63
Table 6: Main properties of hub and nacelle	64
Table 7: Main structural properties of the blades.....	64
Table 8: Standard signals that are written to the shared memory by Flex5 during time domain simulations.....	66
Table 9: Distributed geometrical properties of the tower for use with the monopile. h is the vertical distance of a cross section from tower bottom, D the outer diameter, and t the wall thickness.....	68
Table 10: Sensors defined for the monopile substructure	68
Table 11: Dimensions of the tripod members.....	69
Table 12: Main properties of the OC3 tripod model.....	69
Table 13: Distributed geometrical properties of the tower. h is the vertical distance of a cross section from tower bottom, D the outer diameter, and t the wall thickness.....	70
Table 14: Sensor locations and description for member force sensors defined for the tripod support structure.....	71
Table 15: Main properties of the jacket	74
Table 16: Load cases investigated for Phase I of the OC3 project.....	86
Table 17: Coupled system eigenfrequencies calculated by Flex5-Poseidon for Phase I system.....	87
Table 18: Load cases investigated for Phase III of the OC3 project.....	98
Table 19: Coupled system eigenfrequencies calculated by Flex5-Poseidon for Phase III	99
Table 20: Static axial forces including buoyancy effects at sensor locations 1-6.....	100
Table 21: Static fore-aft shear forces including buoyancy effects at sensor locations 1-6	100

Table 22: Static fore-aft bending moments including buoyancy effects at sensor locations 1-6	100
Table 23: Coupled system eigenfrequencies for the jacket	104
Table 24: Recommended marine growth thickness depending on water depth and region	108
Table 25: Coupled system eigenfrequencies taking hydrodynamic added mass into account	110
Table 26: Coupled system eigenfrequencies taking hydrodynamic added mass and local joint flexibility into account	120
Table 27: Local eigenfrequencies with fixed interface node	130
Table 28: Load case groups for comparative calculations.....	131
Table 29: Wind speeds and sea state parameters for combined wind and wave loading in LC3.xx and for wave loads in LC4.xx	132
Table 30: Keypoint numbers and coordinates for the jacket model	154
Table 31: Line definitions for the jacket model	156
Table 32: Material definition for the jacket model	159

List of Figures

Figure 1: Parts of an offshore wind turbine, taken from IEC 61400-3	xvii
Figure 2: Offshore wind turbines and support structures used for the offshore test field <i>alpha ventus</i> . Multibrid M5000 on a tripod support structure (left); REpower 5M on a jacket (right).....	2
Figure 3: Applicability of regular wave theories, taken from IEC 61400-3.....	9
Figure 4: Wheeler stretching (taken from DNV-RP-C205).....	10
Figure 5: Comparison of PM and JONSWAP wave energy spectrum for $H_s = 4\text{m}$ and $T_z = 8\text{s}$	12
Figure 6: Illustration of the difference in the appearance of the sea surface for a linear wave (a), unidirectional sea state (b), and sea state with a spreading function applied (c)	13
Figure 7: Scatter diagram for the north sea.....	13
Figure 8: Types of loads and the respective causes	18
Figure 9: Dynamic amplification function V for different damping ratios D	20
Figure 10: Ratio of amplification factors V_1/V_2 for different ratios of natural frequencies ω_1/ω_2 and different damping ratios.....	20
Figure 11: Exemplary Campbell Diagram for first global eigenfrequency	21
Figure 12: Schematic illustration of the superposition method	28
Figure 13: Schematic flow chart of the analysis procedure for the semi-integrated approach	29
Figure 14: Schematic flow chart for the sequential approach	30
Figure 15: Schematic flow chart for the full coupling approach.....	31
Figure 16: Schematic of calculation of rigid body forces for a trapezoidal distributed load within an element	39
Figure 17: Screenshot of Poseidon's visualization of the structural model of the research platform FINO1; model (left), mesh with first eigenmode (middle), and 3D-visualization (right).....	40
Figure 18: Plot of wave load on monopile structure. The mudline level can be specified arbitrarily, structural information and loads remain the same.	41
Figure 19: Airy wave loads on a monopile. View of the model with keypoints and lines (left); view of the mesh with nodes and elements (right).	42

Figure 20: Pressure vectors on an inclined conical member with diameter D	42
Figure 21: Illustration of the effect of solving the first step statically compared to dynamic solution even for the first step	47
Figure 22: Screen shot of the TimeHistoryTool in Poseidon.....	49
Figure 24: Coupling scheme on matrix level for the full coupling of Flex5 and Poseidon system matrices; schematic matrix symbolizes Flex5's full mass matrix.....	52
Figure 25: Schematic illustration of the global stiffness and damping matrix. Flex5's stiffness and damping matrices are diagonal matrices.	53
Figure 26: Comparison of Flex5's foundation coordinate system with Poseidon's global coordinate system	54
Figure 27: Schematic diagram of the time domain simulation procedure	58
Figure 28: Poseidon model of the monopile support structure.....	67
Figure 29: Tripod model.....	69
Figure 30: Tripod model with keypoint numbers (left) and line numbers (right) (referred to as node and member numbers in Table 14)	71
Figure 31: 3D-visualization of the jacket model.....	73
Figure 32: Sensor locations for the jacket	75
Figure 33: Wind speed at hub height for mean wind speed $v_{hub} = 8$ m/s and turbulence intensity $I_T = 14\%$	76
Figure 34: Comparison of bending moments at mudline for a vertical monopile loaded by an Airy wave with $H=0.5$ m, $T=5.5$ s, and water depth $d=30$ m. Loads have been calculated with Poseidon, WaveSim/ANSYS, and STAAD, respectively.....	78
Figure 35: Comparison of bending moments at mudline for an inclined monopile loaded by an Airy wave with $H=1.01$ m, $T=5.07$ s, and water depth $d=30$ m. Loads have been calculated with Poseidon, WaveSim/ANSYS, and STAAD, respectively.....	78
Figure 36: Comparison of analytical and simulated power density spectrum of the sea surface elevation for a sea state with $H_s=4$ m and $T_z=8$ s.	79
Figure 37: Research platform FINO 1. a) Locations of strain gages. b) Numerical model and orientation with respect to nautical North	80
Figure 38: Five lowest eigenfrequencies of the Poseidon model of the FINO1 platform with according mode shapes.....	81
Figure 39: FFT of the measured axial force at the detail BDSW for a sea state with $H_s=3$ m, $T_z=6$ s, mean direction 225 deg.	82
Figure 40: Comparison of simulated vs. measured damage equivalent axial forces at the detail BDSW for two different sea states from different directions (225° in light grey, 315° dark grey)	83
Figure 41: Schematic overview of lumped masses of the RNA	84
Figure 42: Axial force at tower top for $v_{hub} = 0$ m/s	84

Figure 43: Fore-aft bending moment at tower top for $v_{hub} = 0\text{m/s}$	85
Figure 44: Comparison of the coupled modal analysis results in Phase I.....	88
Figure 45: Blade 1 in-plane bending moment at the blade root (top), rotor speed (bottom) for load case 3.1	89
Figure 46: Rotor torque for load case 3.1.....	89
Figure 47: Mudline fore-aft bending moment (top) and rotor thrust at yaw bearing level (bottom) for load case 3.1.....	90
Figure 48: Power spectra of the in-plane (top) and out-of-plane bending moment (bottom) at the root of blade 1 for load case 3.2	91
Figure 49: Power spectra of mudline fore-aft shear force (top) and bending moment (bottom) for load case 3.2	92
Figure 50: Fore-aft shear force (top) and bending moment (bottom) at mudline for load case 4.1	93
Figure 51: Fore-aft shear force (top) and bending moment (bottom) at mudline for load case 4.3	94
Figure 52: Power spectra of the fore-aft shear force (top) and bending moment at mudline for load case 4.2.....	95
Figure 53: Sensor locations for comparison of structural simulation results	98
Figure 54: Comparison of the coupled modal analysis results in Phase I.....	99
Figure 55: Member forces at location 4 (upwind upper diagonal) in load case 4.3	101
Figure 56: Determination of eigenfrequencies of a simple beam.....	103
Figure 57: First local brace modes of the jacket.....	105
Figure 58: Influence of the boundary constraints. Left: rotations at supports allowed; right: supports fully rigid.	106
Figure 59: Hydrodynamic added mass compared to unit weight of tubulars vs. diameter	107
Figure 60: Marine growth added mass compared to hydrodynamic added mass and steel unit weight.	108
Figure 61: Local brace modes of the jacket with hydrodynamic added mass	111
Figure 62: Comparison of support structure modes coinciding with the 2 nd collective edgewise bending mode for different modeling conditions. Left: reference case without hydrodynamic mass resulting in no coupling between local jacket dynamics and edgewise blade bending. Right: Situation with hydrodynamic added mass resulting in coupling between side-to-side vibrations of braces and edgewise (side-to-side) blade bending. (Same displacement scaling for both plots.).....	112
Figure 63: Participation factors for the DOFs of the RNA for the mode displayed in Figure 62	112
Figure 64: T-joint modelled with beam elements.....	113

Figure 65: FE-model of a T-joint showing the local deformation of the shell surface.....	114
Figure 66: Definition of geometric properties and loading of tubular joints ..	115
Figure 67: Modeling of LJF using beam elements with adapted stiffness properties.....	116
Figure 68: Assembly of the super-element in the beam model.....	117
Figure 69: Jacket model with rigid and flex elements according to the Buitrago approach.....	119
Figure 70: Normalized top deformations of a submerged pole in free vibration with different initial deformations.....	122
Figure 71: Two-degree-of-freedom system with two masses and two springs	123
Figure 72: Ratio of the eigenfrequencies calculated analytically and with generalized stiffness and mass for the two mass oscillator for different spring stiffness ratios k_2/k_1	125
Figure 73: Example system	126
Figure 74: First global fore-aft mode (left) and local fore-aft mode of the cantilever (right)	126
Figure 75: Local fore-aft frequency of the cantilever sub-component with fixed interface node.....	127
Figure 76: Power spectral density of the fore-aft bending moment at the cantilever root.....	128
Figure 77: Example system with harmonic excitation force (left) and resulting time series of fore-aft bending moment for full and sequential approach and $\eta_1=0.95$	129
Figure 78: Example system with harmonic excitation force (left) and resulting time series of fore-aft bending moment for full and sequential approach and $\eta_1=1.05$	129
Figure 79: Campbell diagram for the jacket model with rotor speeds for different wind speeds and potential sources of resonance.....	133
Figure 80: Normalized PSDs of the axial force in the leg at mudline for LC1.07 and LC1.09	134
Figure 81: Normalized PSDs of the keypoint accelerations due to out-of-plane vibration of the braces in the lowest bay for LC1.09. Top: downwind face of the jacket; bottom: side face of the jacket.....	135
Figure 82: Normalized PSDs of the keypoint accelerations due to out-of-plane vibration of the braces in the lowest bay for LC1.13. Top: downwind face of the jacket; bottom: side face of the jacket.....	136
Figure 83: Normalized PSD of the axial force in the downwind leg of the jacket at mudline	137
Figure 84: Rotor speed in LC2.09 for the time interval that has been used for the FFT.....	137

Figure 85: Out-of-plane accelerations of the braces in the first bay; harmonic excitation frequency ranges with varying rotor speed (between 10.4 and 11.3 rpm)	138
Figure 86: Normalized PSD of the out-of-plane vibration of the downwind brace in the second bay for 13m/s, harmonic excitation frequency ranges with varying rotor speed (between 11.8 and 12.5 rpm).....	138
Figure 87: Normalized PSDs of the out-of-plane acceleration of the downwind brace in the first bay for LC3.13 (top) and LC3.23 (bottom).....	139
Figure 88: Acceleration of the side-face brace in the first bay for LC3.23....	140
Figure 89: Normalized PSD for the out-of-plane displacement of the brace in the first bay.....	140
Figure 90: DEL ratios $DEL_{full}/DEL_{sequential}$ for the axial forces in the legs of the jacket.....	141
Figure 91: DEL ratios $DEL_{full}/DEL_{sequential}$ for the out-of-plane shear forces in the downwind braces of the jacket.....	142
Figure 92: Comparison of the PSDs of the out-of-plane shear force at the downwind brace in bay 1	142
Figure 93: Comparison of time histories for the out-of-plane shear force in the downwind bracing in the first bay	143
Figure 94: Rainflow spectra for the out-of-plane shear force in the downwind bracing in the first bay.....	143
Figure 95: Average DEL ratios for all sensors of the reference jacket substructure (sensor names not shown explicitly for clarity)	145
Figure 96: Numbering scheme for keypoints and lines.....	154
Figure 97: Coordinate system and angles of rotation for coordinate transformation of two-noded line elements	161

Nomenclature

Acronyms and Abbreviations

acc.	according
BEM	Blade-element-momentum theory
cf.	confer
COG	Centre of gravity
DEL	Damage equivalent load
DIBt	Deutsches Institut für Bautechnik
DOF	Degree of freedom
FE / FEM	Finite element method
FFT	Fast Fourier Transform
IEC	International Electrotechnical Commission
LAT	Lowest astronomical tide
MSL	Mean sea level
NREL	National Renewable Energy Laboratory, USA
NTM	Normal turbulence model
NWP	Normal wind profile
OC3	Offshore Code Comparison Collaborative
OWT	Offshore wind turbine
PSD	Power spectral density
RCM	Rainflow counting method
RNA	Rotor nacelle assembly
SWE	Endowed Chair of Wind Energy, University of Stuttgart
GL	Germanischer Lloyd
GH	Garrad Hassan and Partners Ltd.
IEA	International Energy Agency
eq. / eqs.	Equation / Equations
RISØ	National Laboratory for Sustainable Energy at the Technical University of Denmark
IWES	Fraunhofer Institute for Wind Energy and Energy System

	Technology
CWMT	Fraunhofer Center for Wind Energy and Marine Technology
LUH	Leibniz Universität Hannover
DTU	Technical University of Denmark
SCADA	Supervisory Control And Data Acquisition

Symbols

a	[-]	longitudinal flow induction factor
a'	[-]	tangential flow induction factor
a_s	[m/s ²]	structural acceleration normal to the member
a_w	[m/s ²]	water particle acceleration normal to the member
C_a	[-]	hydrodynamic added mass coefficient
C_D	[-]	aerodynamic drag coefficient
C_d	[-]	hydrodynamic drag coefficient
C_L	[-]	aerodynamic lift coefficient
C_m	[-]	hydrodynamic inertia coefficient
d	[m]	water depth
D	[m]	diameter of a tubular structural member
H_s	[m]	significant wave height
I	[-]	turbulence intensity
I_{ref}	[-]	reference turbulence intensity acc. to IEC 61400
m_n		n-th spectral moment of a stochastic process
t	[m]	wall thickness of a tubular structural member
T_p	[s]	peak period
T_z	[s]	zero-up-crossing period
$v(z)$	[m/s]	mean wind speed at height z
$v(z_{ref})$	[m/s]	mean wind speed at reference height z_{ref}
v_{hub}	[m/s]	10-minute mean wind speed at hub height
v_{ave}	[m/s]	annual mean wind speed at hub height
v_{in}, v_{out}	[m/s]	cut-in, cut-out wind speed
v_r	[m/s]	relative velocity of the flow normal to the member surface
u_{10}	[m/s]	hourly mean wind speed at 10m above sea surface
z	[m]	height coordinate
z_{ref}	[m]	reference height for definition of wind profile

γ	[-]	shape parameter for the JONSWAP spectrum
η	[m]	water surface elevation
σ_1	[m/s]	standard deviation of wind speed
α	[-]	wind shear exponent
V	[-]	dynamic amplification factor/function
η	[-]	frequency ratio
Ω	[rad/s]	excitation frequency
ω	[rad/s]	natural frequency
D	[-]	damping ratio

Parts of an Offshore Wind Turbine according to IEC 61400-3

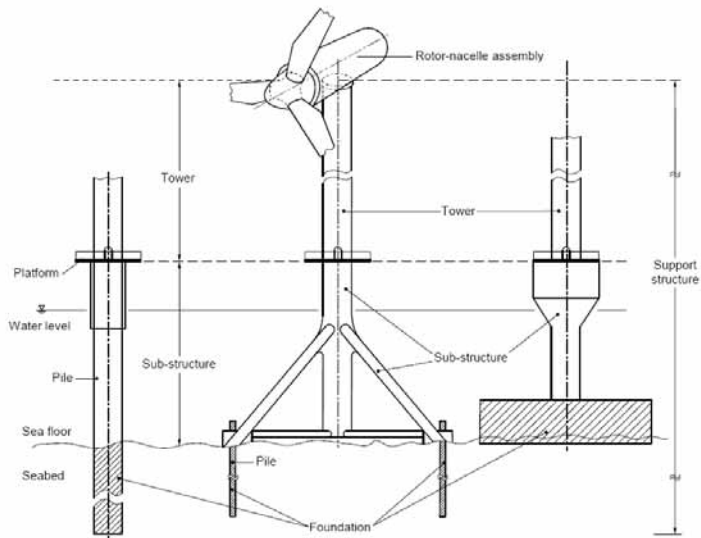


Figure 1: Parts of an offshore wind turbine, taken from IEC 61400-3